HIGH RESOLUTION SIMULATIONS OF THE MARTIAN ATMOSPHERE WITH A GENERAL CIRCULATION MODEL.

Y. O. Takahashi, Y.-Y. Hayashi, M. Odaka, *Division of Earth and Planetary Sciences, Hokkaido University, Japan (yot@ep.sci.hokudai.ac.jp)*, **W. Ohfuchi,** *The Earth Simulator Center, Japan Agency for Marine-Earth Science and Technology, Japan*.

Introduction

A number of numerical simulations of the Martian atmosphere have been performed so far by using general circulation models (GCMs) [e.g., *Haberle et al.*, 1999; *Wilson and Hamilton*, 1996; *Forget et al.*, 1999], and mesoscale and/or convection resolving models [e.g., *Odaka*, 2001; *Rafkin et al.*, 2001; *Toigo and Richardson*, 2002] to investigate atmospheric phenomena of the various scales. In recent years, multiscale modeling which covers both large and small scales simultaneously has been attempted. By the use of a nested model, *Moudden and Mcconnell* [2005] performed a global scale simulation to investigate generation of atmospheric disturbances caused by mountains. Our attempt here is to use a GCM but with the higher resolutions compared to the former studies to investigate the medium scale disturbances, whose horizontal scales range from thermal convection to baroclinic waves. An advantage of using a high resolution GCM compared to a nested model is that we can simulate small and medium scale disturbances over the whole globe under the condition of a consistent global scale circulation, and vice versa. High resolution GCM simulations may provide some insights into dust cycle in the Martian atmosphere, since the medium scale disturbances may have important roles on atmospheric dust lifting and transport.

Recently, we have started new GCM simulations with the aid of the Earth Simulator (ES) and the AFES, an efficient Earth's atmospheric GCM for the ES. Up to now, we have modified the AFES for Mars simulations and performed several simulations with the moderate resolutions of triangular truncation at the total wavenumber of 79 and 159 (T79 and T159, that correspond to $\sim$90, 45 km grid sizes, respectively). We are preparing for the higher resolution simulations at the moment. In this talk, the outline of the Mars GCM based on the AFES used for the high resolution simulations is presented. In addition, some preliminary results on the atmospheric circulations and the dust lifting/transport processes simulated by the model are described.

Model description

The Mars GCM used in this study has been developed by combining the dynamical core of AFES [*Ohfuchi et al.*, 2004] and the physical processes implemented in our Mars GCM [*Takahashi et al.*, 2003, 2004, 2006]. The AFES is a spectral Eulerian primitive equation model with a traditional sigma vertical coordinate. Its original code was adopted from the version 5.4.02 of an atmospheric GCM developed jointly by the Center for Climate System Research (CCSR) of the University of Tokyo and the Japanese National Institute for Environmental Studies (NIES) [*Numaguti et al.*, 1997]. The AFES is optimized to perform high resolution simulations of the Earth's atmosphere on the ES efficiently. The first 10-km mesh global simulation of the Earth's atmosphere was successfully performed by using the AFES.

The physical processes introduced from our Mars GCM are the radiation, the turbulent mixing, and the surface processes. The atmospheric mass change accompanying the formation of CO_2 polar caps is also considered. These are the same as those used in the simulations performed to investigate the topographic effects on the meridional circulation [*Takahashi et al.*, 2003] and the structure of migrating diurnal tide in the Martian atmosphere [*Takahashi et al.*, 2006], and are summarized as follows. The radiation scheme treats absorption by CO_2 gas, and absorption and scattering by dust suspended in the atmosphere. The turbulent mixing is evaluated by using a simplified Mellor and Yamada [1982] level 2.5 scheme, in which the advection of eddy kinetic energy is neglected. The surface topography and albedo variation are based on the Mars Global Surveyor (MGS) observations [Smith et al., 1999; Christensen et al., 2001]. The distribution of soil thermal inertia specified in the model is the same as that used by *Pollack et al.* [1990].

In this study, dust is treated as a radiatively active tracer and its lifting process at the surface is considered. The dust lifting process implemented in our model is the same as "threshold-sensitive surface stress lifting" parameterization described by *Newman et al.* [2002]. Dust is lifted only when the surface friction velocity evaluated by the model-resolved winds exceeds a certain threshold value; the effects of subgrid scale disturbances are not considered in this parameterization. In addition, it is assumed that dust is lifted only on the ice-free surface. The advection of dust is evaluated by a semi-Lagrangian tracer transport scheme that is newly implemented in this study, instead of the spectral scheme used in the usual AFES simulations.

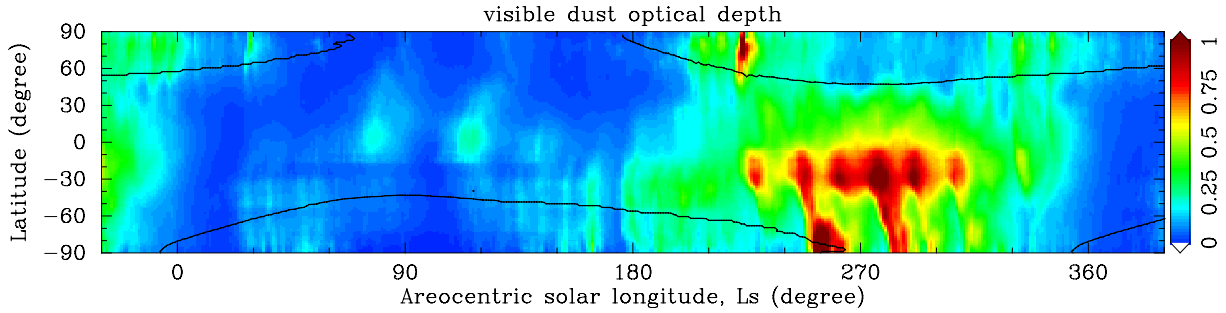

Figure 1: Annual variation of latitudinal distribution of zonal mean dust optical depth. Also shown is the location of polar cap edge (solid line).

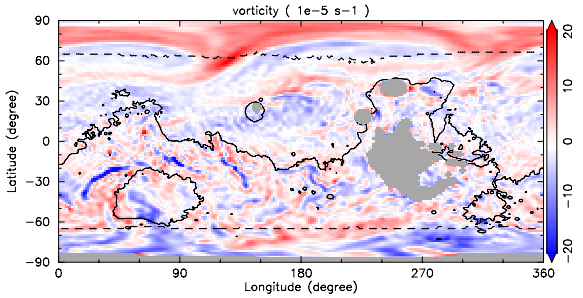

Figure 2: An example of the global vorticity distribution at a 4 hPa pressure level at the northern fall (L_s = 211°). Also shown are the areoid (solid line) and the location of polar cap edge (dashed line). Gray areas represent mountains at the 4 hPa pressure level.

Results

In the followings, we will describe some results obtained by our simulation with T79 horizontal resolution. In this simulation, the upper most model layer is located at about 90 km altitude, and the model vertical domain is divided into 48 layers. The initial condition is taken from a long term simulation result with the T39 horizontal resolution, that corresponds to ∼180 km grid size. The T79 simulation is performed for about two Martian years and first year data are used for analysis.

Figure 1 shows an annual variation of latitudinal distribution of zonal mean dust optical depth simulated by our model. The dust optical depth is large in the northern fall, winter, and spring, whereas it is small in the northern summer. This annual variation is roughly consistent with observed one. However, the dust optical depth in the northern winter is larger than observed one and its annual variation is repeated in the next year almost in the same way (not shown here).

Hereafter, we will focus on the behavior of the atmosphere in the northern fall when the dust optical depth increases. Figure 2 shows an example of global vorticity distribution at a 4 hPa pressure level at L_s = 211°. The vorticity disturbance with zonal wavenumber two appears in the northern high latitude region. This disturbance propagates eastward and is considered to be a baroclinic wave. Associated with this wave, a front is observed clearly as a narrow tail-like structure of vorticity. The frontal structure like this is generated in two preferential longitudinal regions; the Utopia (∼80°E–140°E) and the Acidalia (∼280°E–360°E).

In the lees of several high mountains in the northern hemisphere, medium scale vortices appear. The typical regions are the Elysium (150°E, 25°N), the Olympus (230°E, 20°N), and the Alba Patera (250°E, 40°N). Figure 3 shows composite distributions of vorticity around the Alba Patera at the northern fall (L_s = 210°–240°). In the lees of high mountains including the Alba Patera, the vortex pairs are generated periodically with a period of one sol. It seems that the mean wind and the diurnally varying circulation around the high mountains cause these periodic vortex generation.

In the southern hemisphere, a number of vortices and narrow shear zones are observed. A typical example is shown as a vorticity filament at around 30°E and 30°S in Figure 2. A sensitivity experiment without surface topography implies the importance of local topographic variation in generating these features. The topographic variation in the southern hemisphere seems to play an important role in generating these disturbances over the wide area of the hemisphere.

Figure 4 shows distributions of dust mass flux and dust optical depth scaled to a 6.1 hPa pressure level at the same time as Figure 2. In Figure 4a, it is shown that dust is lifted in the frontal region shown in Figure 2. The dust lifted in the frontal region is advected along the front and results in an "elongated dust storm" as shown in Figure 4b. The dust storms of this shape are frequently observed by Mars Orbiter Camera (MOC) onboard the MGS spacecraft and are referred to as a "flushing dust storm" or a "frontal dust storm" [*Wang et al.*, 2005]. Our result suggests that the strong wind in fronts plays an important role to lift dust and to generate such dust storms.

Figure 5 shows a geographic distribution of dust

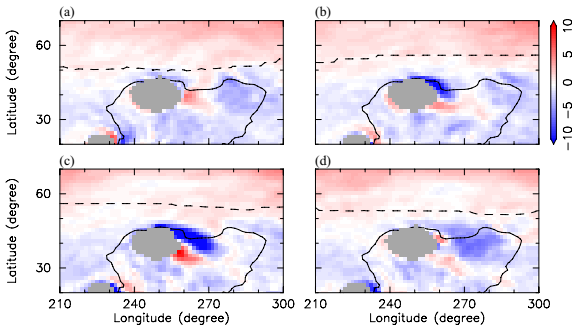

Figure 3: Composite distributions of vorticity around the Alba Patera in the northern fall (L_s = 210°–240°). Panels (a)-(d) show vorticity distributions at the local solar time of 0, 6, 12, and 18 hours at 155°E, respectively. Others are the same as those of Figure 2.

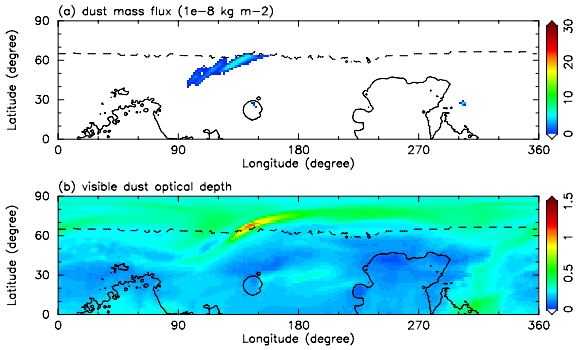

Figure 4: The northern hemispheric distribution of dust mass flux on the ground and dust optical depth scaled to a 6.1 hPa pressure level at the same time as Figure 2. As for dust mass flux, two-hour averaged values are plotted. Also shown are the areoid (solid line) and the location of polar cap edge (dashed line).

mass flux averaged over a period of L_s = 210°–240°. In this season, it is shown that the major dust lifting regions are the Hellas basin (60°E, 50°S), the eastern flank of Tharsis (300°E, 10°S), and the limited longitudinal ranges of the vicinity of northern polar cap, i.e., the Utopia, the north of Alba Patera, and the Acidalia. The result that dust is lifted at the vicinity of polar cap is consistent with MGS observation [*Cantor et al.*, 2001]. Dust lifting in the Utopia and the Acidalia regions is caused by the strong wind in the fronts as shown in Figures 2 and 4. The regions of the Utopia and the Acidalia coincide with the regions where the frontal structure are well developed. These preferential longitudes for dust lifting are considered to appear because of the topographic variation which enhances the activity of baroclinic waves as is described as "storm zones" by *Hollingthworth et al.* [1996].

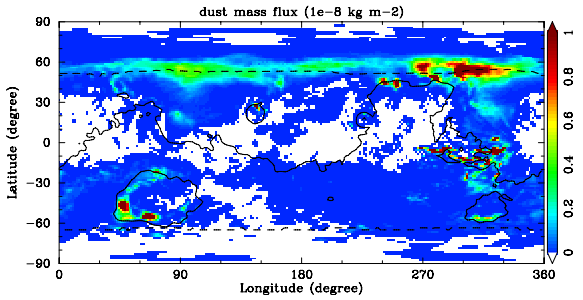

Figure 5: Distribution of dust mass flux averaged over a period of L_s = 210°–240°. Also shown is the areoid (solid line) and the lowest latitude polar cap edge during the period (dashed line).

Concluding remarks

The preliminary results shown above demonstrate that the high resolution simulations are promising to provide new insights into the small and medium scale atmospheric disturbances, and the dust lifting and its transport processes on Mars. Detailed analyses of simulation results are now on going, and we are preparing for simulations with the higher resolution than that shown above.

Acknowledgements

This research has been supported by the Research Fellowships of the Japan Society for the Promotion of Science for Young Scientists. The numerical simulation is performed on the Earth Simulator with support from the Japan Agency for Marine-Earth Science and Technology.

References

Cantor, B. A., P. B. James, M. Caplinger, and M. J. Wolff (2001), Martian dust storms: 1999 Mars Orbiter Camera observations, *J. Geophys. Res.*, *106*, 23653–23687.

Christensen, P. R., J. L. Bandfield, V. E. Hamilton, S. W. Ruff, H. H. Kieffer, T. N. Titus, M. C. Malin, R. V. Morris, M. D. Lane, R. L. Clark, B. M. Jakosky, M. T. Mellon, J. C. Pearl, B. J. Conrath, M. D. Smith, R. T. Clancy, R. O. Kuzmin, T. Roush, G. L. Mehall, N. Gorelick, K. Bender, K. Murray, S. Dason, E. Greene, S. Silverman, and M. Greenfield (2001), Mars Global Surveyor Thermal Emission Spectrometer experiment: Investigation description and surface science results, *J. Geophys. Res.*, *106*, 23823–23871.

Forget, F., F. Hourdin, R. Fournier, C. Hourdin, O. Talagrand, M. Collins, S. R. Lewis, P. L. Read, and J.-P. Huot (1999), Improved General Circulation Models of the Martian Atmosphere from the surface to above 80 km, *J. Geophys. Res.*, *104*, 24155–24175.

Haberle, R. M., M. M. Joshi, J. R. Murphy, J. R. Barnes, J. T. Schofield, G. Wilson, M. Lopez-Valverde, J. L. Hollingsworth, A. F. C. Bridger, and J. Schaeffer (1999), General Circulation Model Simulations of the Mars Pathfinder Atmospheric Structure Investigation/Meteorology Data, *J. Geophys. Res.*, *104*, 8957–8974.

Hollinsworth, J. L., R. M. Haberle, J. R. Barnes, A. F. C. Bridger, J. B. Pollack, H. Lee, and J. Schaeffer (1996), Orographic control of storm zones of Mars, *Nature*, *380*, 413–416.

Newman, C. E., S. R. Lewis, and P. L. Read (2002), Modeling the Martian dust cycle 1. Representation of dust transport processes, *J. Geophys. Res.*, *107*, 5123, doi:10.1029/2002JE001910.

Numaguti, A., S. Sugata, M. Takahashi, T. Nakajima, and A. Sumi (1997), Study on the climate system and mass transport by a climate model, *CGER's Supercomputer Monograph*, *3*, Center for Global Environmental Research, National Institute for Environmental Studies, Tsukuba, Japan.

Mellor, G. L., and T. Yamada (1982), Development of a Turbulent Closure Model for Geophysical Fluid Problems, *Rev. Geophys. Space Phys.*, *20*, 851–875.

Moudden, Y., and J. C. McConnell (2005), A new model for multiscale modeling of the Martian atmosphere, *J. Geophys. Res.*, *110*, E04001, doi:10.1029/2004JE002354.

Odaka, M. (2001), A numerical simulation of Martian atmospheric convection with a two-dimensional anelastic model: A case of dust-free Mars, *Geophys. Res. Lett.*, *28*, 895–898.

Ohfuchi, W., H. Nakamura, M. K. Yoshioka, T. Enomoto, K. Takaya, X. Peng, S. Yamane, T. Nishimura, Y. Kurihara, and K. Ninomiya (2004), 10-km Mesh Meso-scale Resolving Simulations of the Global Atmosphere on the Earth Simulator – Preliminary Outcomes of AFES (AGCM for the Earth Simulator) –, *Journal of the Earth Simulator*, *1*, 8–34.

Pollack, J. B., R. M. Haberle, J. Schaeffer, and H. Lee (1990), Simulations of the General Circulation of the Martian Atmosphere 1. Polar Processes, *J. Geophys. Res.*, *95*, 1447–1473.

Rafkin, S. C. R., R. M. Haberle, and T. I. Michaels (2001), The Mars Regional Atmospheric Modeling System: Model Description and Selected Simulations, *Icarus*, *151*, 228–256.

Smith, D. E., M. T. Zuber, S. C. Solomon, R. J. Phillips, J. W. Head, J. B. Garvin, W. B. Banerdt, D. O. Muhleman, G. H. Pettengill, G. A. Neumann, F. G. Lemoine, J. B. Abshire, O. Aharonson, C. D. Brown, S. A. Hauck, A. B. Ivanov, P. J. McGovern, H. J. Zwally, and T. C. Duxbury (1999), The Global Topography of Mars and Implications for Surface Evolution, *Science*, *284*, 1495–1503.

Takahashi, Y. O., H. Fujiwara, H. Fukunishi, M. Odaka, Y.-Y. Hayashi, and S. Watanabe (2003), Topographically induced north-south asymmetry of the meridional circulation in the Martian atmosphere, *J. Geophys. Res.*, *108*, 5018, doi:10.1029/2001JE001638.

Takahashi, Y. O., M. Odaka, and Y.-Y. Hayashi (2004), Simulations of the Martian climate by the use of general circulation models: their current status and the problems of manipulating dust, Planetary People, 13, 145-155 (in Japanese).

Takahashi, Y. O., H. Fujiwara, and H. Fukunishi (2006), Vertical and latitudinal structure of the migrating diurnal tide in the Martian atmosphere: numerical investigations, *J. Geophys. Res.*, in press.

Toigo, A. D., and M. I. Richardson (2002), A mesoscale model for the Martian atmosphere, *J. Geophys. Res.*, *107*, 5049, doi:10.1029/2000JE001489.

Wang, H., R. W. Zurek, and M. I., Richardson (2005), Relationship between frontal dust storms and transient eddy activity in the northern hemisphere of Mars as observed by Mars Global Surveyor, *J. Geophys. Res.*, *110*, E07005, doi:10.1029/2005/JE002423.

Wilson, R. J., and K. Hamilton (1996), Comprehensive Model Simulation of Thermal Tides in the Martian Atmosphere, *J. Atmos. Sci.*, *53*, 1290–1326.